Computation and characterization of local sub-filter-scale energy transfers in atmospheric flows

Davide Faranda, Valerio Lembo, Manasa Iyer, Denis Kuzzay, Sergio Chibbaro, Francois Daviaud, Berengere Dubrulle

Computation and characterization of local sub-filter-scale energy transfers in atmospheric flows

Davide Faranda[1,2], Valerio Lembo [3], Manasa Iyer[4], Denis Kuzzay[5],

Sergio Chibbaro [4], Francois Daviaud[6] & Berengere Dubrulle[6]

[1]*Laboratoire des Sciences du Climat et de l'Environnement, LSCE/IPSL, CEA-CNRS-UVSQ, Université Paris-Saclay, F-91191 Gif-sur-Yvette, France*

[2] *London Mathematical Laboratory, 14 Buckingham Street, London, WC2N 6DF, UK*

davide.faranda@lsce.ipsl.fr

[3] *Meteorological Institute, University of Hamburg, Grindelberg 5, 20146 Hamburg, Germany*

[4] *Sorbonne Université, UPMC Univ Paris 06, CNRS UMR 7190, Institut Jean le Rond d'Alembert, Paris, France*

[5] *Univ Lyon, Ens de Lyon, Univ Claude Bernard, CNRS, Laboratoire de Physique, F-69342 Lyon, France*

[6] *SPEC, CEA, CNRS, Université Paris-Saclay, CEA Saclay 91191 Gif sur Yvette cedex, France*

*

ABSTRACT

Atmospheric motions are governed by turbulent motions associated to non-trivial energy transfers at small scales (direct cascade) and/or at large scales (inverse cascade). Although it is known that the two cascades coexist, energy fluxes have been previously investigated from the spectral point of view but not on their instantaneous spatial and local structure. Here, we compute local and instantaneous sub-filter scale energy transfers in two sets of reanalyses (NCEP-NCAR and ERA-Interim) in the troposphere and the lower stratosphere for the year 2005. The fluxes are mostly positive (towards subgrid scales) in the troposphere and negative in the stratosphere reflecting the baroclinic and barotropic nature of the motions respectively. The most intense positive energy fluxes are found in the troposphere and are associated with baroclinic eddies or tropical cyclones. The computation of such fluxes can be used to characterize the amount of energy lost or missing at the smallest scales in climate and weather models.

1. Introduction

Large scale atmospheric motions are modeled via a set of nonlinear equations known as primitive equations (Smagorinsky 1963). They include an equation for mass conservation, the thermal energy equation and the evolution equations of velocity fields. The latter are derived from the Navier-Stokes equations on spherical geometry under the hydrostatic assumption, i.e. that vertical motion is much smaller than horizontal motion. Such equations are the cornerstone of all weather and climate models and their explicit implementation depends on the choice of coordinate system and the resolution of the model (Cao and Titi 2007; Klein 2010; Stevens and Bony 2013; Cao et al. 2015). In the classical turbulence phenomenology, valid homogeneous flows, energy is injected at large scales, transferred downscale at a constant averaged rate ε (Kolmogorov (1941) cascade) and dissipated at small scales by viscous effects (Frisch 1995). This phenomenology is based on the so-called Karman-Howarth-Monin (KHM equation), derived directly from the Navier-Stokes equation, that reads:

$$\frac{1}{2}\partial_t E + \varepsilon = -\frac{1}{4}\vec{\nabla}_\ell \cdot \langle \delta\vec{u}(\delta u)^2 \rangle + \nu \nabla_\ell^2 E, \tag{1}$$

where u is the velocity field, ν the molecular viscosity, $\langle\rangle$ means statistical average, ε is the mean non-dimensional energy injection rate, $\delta\vec{u} = \vec{u}(\vec{x}+\vec{\ell}) - \vec{u}(\vec{x})$ is the velocity increments over a distance ℓ and $E(\ell) = \langle(\delta u)^2\rangle/2$ is a measure of the kinetic energy at scale ℓ.

Turbulence in the atmosphere is strongly influenced by density stratification and rotation (Holton and Hakim 2012). Turbulence in such condition is known to develop a complex dynamics, as revealed by accurate numerical simulations and laboratory experiments (Levich and Tzvetkov 1985; Schertzer et al. 1997; Falkovich 1992; Pouquet and Marino 2013). Depending on the scale of the flow, energy transfers can be directed either towards smaller scales (direct cascade) or towards larger scales (inverse cascade) (Bartello 1995). To this aim, Augier et al. (2012) recently consid-

ered a set of primitive equations for incompressible, non-diffusive and inviscid stably stratified fluid in the Boussinesq approximation, in order to account for both the kinetic energy (KE) and available potential energy (APE) in a modified version of the KHM equation. The primitive equations for the stratified Boussinesq fluid were written as:

$$\begin{aligned} \vec{\nabla}\cdot\vec{u} &= 0, \\ \partial_t\vec{u} + \left(\vec{u}\cdot\vec{\nabla}\right)\vec{u} &= -\vec{\nabla}p + b\vec{e}_z + \nu\Delta\vec{u}, \\ \partial_t b + \left(\vec{u}\cdot\vec{\nabla}\right)b &= -N^2 u_z + \kappa\Delta b, \end{aligned} \tag{2}$$

where u is the velocity field,, u_z its vertical component, p the rescaled pressure, ν and κ the viscosity and diffusivity, $N = \sqrt{-(g/\rho_0)(d\bar{\rho}/dz)}$ the constant Brunt-Väisälä frequency, $\mathbf{e_z}$ the vertical unit vector, and $b = -\rho' g/\rho_0$ the buoyancy perturbation, g the acceleration due to gravity, ρ_0 a reference density, $\bar{\rho}(z)$ the mean profile and ρ' a density perturbation. The resulting generalized KHM equation was written as:

$$\begin{aligned} \frac{1}{2}\partial_t E + \varepsilon &= -\frac{1}{4}\vec{\nabla}_\ell \cdot \langle \delta\vec{u}\left[(\delta u)^2 + \frac{(\delta b)^2}{N^2}\right]\rangle, \\ &\equiv \vec{\nabla}\cdot\vec{J}, \end{aligned} \tag{3}$$

where E is now

$$E = \frac{1}{2}\langle(\delta u)^2\rangle + \langle((\delta b)^2/N^2\rangle, \tag{4}$$

and we have omitted contributions due to viscosity and diffusivity. This shows that the flux $\vec{J}$ is made of a KE flux and an APE flux. This equation stems directly from the energy conservation law governing atmospheric dynamics at the dissipative scales. Energy conservation in the atmosphere is clearly described by the Lorenz Energy Cycle (LEC) formulation (Lorenz 1955), showing the conversion of APE into KE and then into dissipative heating. In a spectral sense, the KE and APE fluxes can have different direction, so that the resulting energy flux can be positive, or negative,

depending on the scale, isotropy or stratification, and the corresponding direction of the energy cascade is hard to predict. In other words it is not clear to what extent is applicable a picture of turbulence in a stratified atmosphere in which a clear separation of scales exists between 2-D and 3-D turbulence and whether the two pictures are associated with cascades in opposite directions (Lovejoy and Schertzer 2010).

The lack of general consensus about the direction of cascades also reflects in the interpretation of observational-based results and implementation of turbulence in numerical models. Observed energy spectra in the troposphere and in the lower stratosphere (Nastrom and Gage 1985) exhibit $k^{-5/3}$ law, generally connected to direct cascades, and/or k^{-3} power laws, associated to an inverse energy cascade. The inverse cascade has been historically associated to the quasi-geostrophic two dimensional dynamics induced by rotation (Charney 1971), and fed by baroclinic instability. Tung and Orlando (2003) simulated the Nastrom-Gage energy spectrum of atmospheric turbulence as a function of wavelength with a two-level quasi-geostrophic model, and were able to obtain both spectral behaviours with this simple dynamics. Kitamura and Matsuda (2006) analysed the role of stratification and rotation in the generation of the cascades, observing that in experiments without planetary rotation, the obtained spectral slope was steeper and energy transfer to larger vertical wave-numbers was increased. Some theories for a mesoscale inverse cascade for stratified (not quasi-geostrophic) turbulence were proposed by Gage (1979) and Lilly (1983) but these are no longer considered viable. According to Lindborg (2005), atmospheric mesoscale $-5/3$ energy spectra can be explained by the existence of a direct cascade arising in the limit of strong stratification while the role of planetary rotation is to inhibit the cascade process at large scales leading to an accumulation of kinetic energy and steepening of the kinetic energy spectrum at small wave numbers. Evidence on the existence of a direct energy cascade comes from high resolution direct numerical simulations of stratified flows (Lindborg 2006). They also suggest that the direction of

the cascade may be crucially dependent on the ratio of the Brunt-Väisälä frequency to the rotation frequency.

A way to clarify the situation is to compute the energy fluxes. In the classical picture of turbulence, such energy transfers are related directly to the skewness velocity increments $\langle \delta \mathbf{u} (\delta u)^2 \rangle$, and the direction of the cascade is provided by the sign of this quantity (positive for direct cascade, negative for inverse cascade). This quantity which is global, since it relies on space-average, has thus been used in the past to quantify the direction of the energy transfer. From the observed stratospheric third-order structure function, Lindborg and Cho (2001) argued that there is a forward energy cascade in the mesoscale range of atmospheric motions. In that study the authors pointed out that for scale smaller than 100 km the statistical inhomogeneities can be neglected while this assumption is not valid for larger scales. Similar conclusions also hold for the study of intense phenomena such as in tropical cyclones (Tang and Chan 2015) and suggests that one must be careful in using skewness based approaches to infer energy fluxes depending on the homogeneity assumptions.

Another approach to compute energy fluxes for atmospheric model is to rely on the spectral kinetic energy budgets (see e.g. Augier and Lindborg (2013) and Peng et al. (2015)). However, like the skewness approach, these computations only provide a global in space estimate of the energy transfers and not their local value, nor their instantaneous spatial distribution.

An important breakthrough was made when Duchon and Robert (2000) reformulated the energy budget of the Navier-Stokes equations into a form allowing for the definition of energy transfers local in space and time and valid for any geometry including when strong inhomogeneity and anisotropy are present. Its ability to provide interesting information about energy transfers at a given scale ℓ has been so far exploited in the experimental set-up of the Von Karman swirling flow to measure the scale to scale energy transfers and non viscous energy disipation (Kuzzay et al.

2015; Saw et al. 2016). The Duchon and Robert indicator requires only the 3D velocity fields and provides, for each instant, 3D maps of the sub-filter energy transfers at a scale ℓ. The interest of this formulation is that it is devoid of any adjustable parameters unlike, for exemple, local estimates of energy budgets based on LES methods Kuzzay et al. (2015).

In this work we adapt the definition of such indicators to the atmospheric dynamics providing the first local maps of sub-filter-scale energy transfers without any adjustable parameter. The goal of this work is i) to identify and characterize the atmospheric motions responsible for large energy transfers and ii) to compute global time and spatial average and assess whether the reanalyses over(under)-represent energy fluxes. The paper is structured as follows. After presenting the indicator, we will study these transfers in the NCEP-NCAR and ERA-Interim reanalyses - to ensure that results are model independent - for the year 2005 and investigate: i) the vertical and horizontal global averages, ii) the distribution of energy transfers at different scales, iii) two case studies of intense cyclones that occurred in 2005 (Katrina and Jolina) and also correspond to extreme energy transfers according to our indicator. We finally discuss the implications of our results on a theoretical and practical level.

2. Methods

For any solutions of the Navier-Stokes equations, Duchon and Robert (2000) defined energy transfers in a fluid at an arbitrary scale ℓ using a local energy balance equation

$$\partial_t E^\ell + \partial_j \left(u_j E^\ell + \frac{1}{2}\left(u_j \hat{p} + \hat{u}_j p\right) + \frac{1}{4}\left(\widehat{u^2 u_j} - \widehat{u^2} u_j\right) - \nu \partial_j E^\ell \right) = -\nu \partial_j u_i \partial_j \hat{u}_i - \mathscr{D}_\ell, \qquad (5)$$

where u_i are the components of the velocity field and p the pressure, $\hat{u}$ and $\hat{p}$ their coarse-grained component at scale ℓ, $E^\ell = \frac{\hat{u}_i u_i}{2}$ is the kinetic energy per unit mass at scale ℓ (such that $\lim_{\ell \to 0} E^\ell =$

$u^2/2$), $\mathscr{D}_\ell$ is expressed in terms of velocity increments $\delta\vec{u}(\vec{r},\vec{x}) \stackrel{def}{=} \vec{u}(\vec{x}+\vec{r}) - \vec{u}(\vec{x}) \equiv \delta\vec{u}(\vec{r})$ (the dependence on ℓ and $\vec{x}$ is kept implicit) as:

$$\mathscr{D}_\ell(\vec{u}) = \frac{1}{4\ell}\int_{\mathscr{V}} d\vec{r}\ (\vec{\nabla}G_\ell)(\vec{r})\cdot\delta\vec{u}(\vec{r})\ |\delta\vec{u}(\vec{r})|^2, \tag{6}$$

where G is a smooth filtering function, non-negative, spatially localized and such that $\int d\vec{r}\ G(\vec{r}) = 1$. The function G_ℓ is rescaled with ℓ as $G_\ell(\vec{r}) = \ell^{-3}G(\vec{r}/\ell)$. As shown in Duchon and Robert (2000), the choice of G has no impact on the value of $\mathscr{D}_\ell$, in the limit $\ell \to 0$, as long as it satisfies the properties specified previously. In the sequel, we therefore choose a spherically symmetric function of x given by:

$$G_\ell(r) = \frac{1}{N}\exp(-1/(1-(r/(2\ell)^2)), \tag{7}$$

where N is a normalization constant such that $\int d^3r G_\ell(r) = 1$.

As noticed by Duchon and Robert, the average of $\mathscr{D}_\ell(\vec{u})$ can be viewed as a weak form of the transfer term $-\frac{1}{4}\vec{\nabla}_\ell\cdot\langle\delta\vec{u}(\delta u)^2\rangle$ in the anisotropic version of the KHM equation Eq. (1), the divergence being taken not on the term itself, but instead on the test function G_ℓ. Without taking the average, we see then that $\mathscr{D}_\ell(\vec{u})$ is a local energy transfer, the sign of which provides the direction of the fluxes in the scale space: a positive sign implies transfer towards the scales smaller than ℓ.

By construction, the intrinsic weak formulation of $\mathscr{D}_\ell(\vec{u})$ makes it less sensitive to noise than classical gradients, or even than the usual KHM relation: indeed, the derivative in scale is not applied directly to the velocity increments, but rather on the smoothing function, followed by a local angle averaging. This guarantees that no additional noise is introduced by the procedure. Even more, the noise coming from the estimate of the velocity is naturally averaged out by the angle smoothing as shown in Kuzzay et al. (2015). In the same study, the authors argued that the

Duchon and Robert approach was a better alternative to the widespread large eddies simulation based method for the computation of energy fluxes, since it relies on very few arbitrary hypotheses. Experimentally, in the von Karman set-up, the DR formula provided a better estimate of the energy dissipation than a LES method: in particular, estimates of the injected and dissipated powers were within 20% of the measured value using the LES-PIV method, whereas reached 98% of the actual dissipation rate of energy with the DR formula Kuzzay et al. (2015).

In order to use this approach for atmospheric dynamics requires taking into account density stratification, and considering Boussinesq equations instead of Navier-Stokes equations. We have adapted the Duchon-Robert formalism to the Boussinesq equations. The equation for the kinetic energy is simply restated as

$$\partial_t E^\ell + \vec{\nabla}\cdot\vec{J}^\ell_K = -\nu\partial_j u_i \partial_j \hat{u}_i - \mathscr{D}_\ell + \frac{1}{2}\left(b\hat{u}_z + \hat{b}u_z\right). \tag{8}$$

Using the point-split buoyancy perturbation as fundamental variable, we can then obtain an equation related to the local variance of the buoyancy perturbation(details are given in the appendix)

$$\partial_t E^\ell_T + \vec{\nabla}\cdot\vec{J}^\ell_T = -\mathscr{D}^T_\ell - \frac{1}{2}\left(b\hat{u}_z + \hat{b}u_z\right) - \kappa\partial_j\hat{b}\partial_j b/N^2\ , \tag{9}$$

where $E^\ell_T = \frac{\hat{b}b}{2N^2}$ is the available potential energy at scale ℓ, $\mathscr{D}^T_\ell$ is expressed in terms of the increments $\delta b(\vec{r},\vec{x}) \overset{def}{=} b(\vec{x}+\vec{r}) - b(\vec{x}) \equiv \delta b(\vec{r})$ (the dependence on ℓ and $\vec{x}$ is kept implicit) as

$$\mathscr{D}^T_\ell = \frac{1}{4\ell}\int_{\mathscr{V}} d\vec{r}\ (\vec{\nabla}G_\ell)(\vec{r})\cdot\delta\vec{u}(\vec{r})\ |(\delta b)|^2/N^2. \tag{10}$$

Considering now that the energy for stratified flows is given by expression (4), we can sum equation (8) and (9), to get the total local energy balance

$$\partial_t E^\ell + \vec{\nabla}\cdot\vec{J}^\ell = -\mathscr{D}_\ell(\vec{u},b) - \nu\partial_j\hat{u}_i\partial_j u_i - \kappa\partial_j\hat{b}\partial_j b/N^2, \tag{11}$$

where

$$\vec{J}^\ell = \vec{J}^\ell_K + \vec{J}^\ell_T, \tag{12}$$

is the spatial energy flux, and

$$\mathscr{D}_\ell(\vec{u},b) = \frac{1}{4\ell}\int_{\mathscr{V}} d\vec{r}\,(\vec{\nabla}G_\ell)(\vec{r})\cdot\delta\vec{u}\left[(\delta u)^2 + \frac{(\delta b)^2}{N^2}\right], \tag{13}$$

is the total local scale to scale energy flux. It is easy to see that the average of $\mathscr{D}_\ell(\vec{u},b)$ is a weak formulation of the energy transfer terms of the generalized KHM equation of Augier et al Eq. (3). The DR indicator $\mathscr{D}_\ell(\vec{u},b)$ is thus a local energy transfer term, that can be split into a kinetic (dynamical) part $\mathscr{D}_\ell(\vec{u})$ (the original DR indicator) and a potential (thermodynamic) part (the remaining part, implying the field b). In order to easily implement the expression of $\mathscr{D}_\ell(\vec{u},b)$ in climate models, the buoyancy parameter has been rewritten as a function of temperature T using the equation of state fro dry air: $\delta b = -\delta p/\rho_0 R\cdot 1/\delta T$, where ρ_0 is a reference density at surface pressure and δp is a pressure horizontal perturbation, which is set to be about 10 hPa each 100 km. Furthermore, in Eq. 13, we set a constant Brunt-Väisälä frequency, amounting to 1.2×10^{-1} s^{-1} Holton and Hakim (2012), is chosen. In this way, the computation of $\mathscr{D}_\ell(\vec{u},b)$ only requires the numerical 3D velocity u and T fields.

The sign and geometry of the zones associated with high and low values of $\mathscr{D}_\ell(\vec{u},b)$ will then provide interesting information about the dynamics of the energy exchange in the atmosphere. For example, a study of the occurrence of high and low values of $\mathscr{D}_\ell(\vec{u})$ in the von Kármán swirling flow has revealed that such events are associated with well defined, characteristic geometry of the velocity field Saw et al. (2016). For the kinetic (dynamical) part, positive values of $\mathscr{D}_\ell(\vec{u})$ are measured whenever there is a strong convergence of the flow. Divergent flows are instead associated to negative values of $\mathscr{D}_\ell(\vec{u})$, and they point to injection of energy from the sub-filter scales. This simple description is not valid anymore when we also consider the potential (thermodynamic) component. For all these reasons, we cannot reduce the computation of $\mathscr{D}_\ell(\vec{u})$ to only that of the

194 divergence/vorticity. As we will see in Section 3.1 for real atmospheric flows, dipolar $\mathscr{D}_\ell(\vec{u},0)$
195 structures may appear with 3D structures as those observed during hurricanes.

196 3. Analysis

197 For this study, outputs of the ERA-Interim and NCEP-NCAR Reanalysis 1 have been
198 used. ERA-Interim is the currently operational Reanalysis product at the European Center for
199 Medium-Range Weather Forecasting (ECMWF) (Dee et al. 2011). Released in 2007, it provides
200 reanalyzed data from 1979 to nowadays, stored at an original T255 spectral resolution (about
201 80 km horizontal resolution), with 60 vertical hybrid model levels. A 12h four-dimensional
202 variational data assimilation (4D-Var) is adopted. As a forecast model, the Integrated Forecast
203 Model (IFS), Cy31r2 release, is used, fully coupling modules for the atmosphere, ocean waves
204 and land surface. Sea-surface temperatures (SST) and sea-ice concentration (SIC) are ingested
205 as boundary conditions and interpolated on a reduced-Gaussian grid as needed. In our case
206 zonal, meridional and vertical wind components are considered at a $0.75^\circ \times 0.75^\circ$ horizontal
207 resolution over 12 pressure levels between 1000 and 100 hPa. A 12h time-step is considered.
208 Known problems concerning these datasets are the lack of dry mass conservation (Berrisford et al.
209 2011) and the slight asymmetry between evaporation and precipitation (Dee et al. 2011). The
210 turbulent fluxes are based on the tiled ECMWF scheme for surface exchanges over land (Viterbo
211 and Beljaars 1995; Viterbo and Betts 1999). Each gridbox is divided into up to six fractions
212 (over land) depending on the type of surface, having different transfer coefficients based on a
213 Monin-Obukhov formulation. Similarly, over oceans, two different coefficients are used for stable
214 and unstable conditions (Beljaars 1995).
215

NCEP-NCAR Reanalysis 1 has been developed in a joint effort by the National Center for Environmental Prediction (NCEP) and the National Center for Atmospheric Research (NCAR) (Kalnay et al. 1996). The simulation is operational since January 1995, covering a period from 1948 to nowadays. Data assimilation is performed via a 3D variational scheme (Parrish and Derber 1992). The NCEP model system, operational in 1994, has been used for forecasting. It features a T62 spectral resolution, corresponding to a $2.5^\circ \times 2.5^\circ$ horizontal grid (about 200 km horizontal resolution), with 28 sigma levels. Most of the major physical processes involving the climate system are parametrized. SST, SIC, snow cover, albedo, soil wetness and roughness length are ingested as boundary conditions. Data are archived at an original 6h time-step, and such a temporal resolution is retained for our analysis. The atmospheric model which provides the NCEP/NCAR reanalysis data, uses bulk aerodynamic formulas to estimate the turbulent fluxes, with exchange coefficients depending on empirical profiles extending the Monin-Obukhov similarity relationship (Miyakoda and Sirutis 1986). For more details on the comparison between different subgrid parametrization of surface fluxes, one might refer to Brunke et al. (2011).

a. Analysis of local energy transfers

1) YEARLY AND SEASONAL AVERAGE LOCAL ENERGY TRANSFERS

We begin the analysis by studying the latitudinal averages and the spatial features of the DR indicator for both the ERA-Interim reanalysis and the coarser NCEP-NCAR reanalysis. To enable comparison between the two datasets, one has to choose the analysis length larger than the resolution scale of NCEP-NCAR (200km) since going below the resolution size introduces spurious effects dependent on the filter design. On the other hand, since we want to have as much details as possible, we have to choose the smallest scale consistent with those requirements. Here, we thus

adopt a scale of $\ell = 220$ km, this scale being the smallest that provide reliable estimates of DR indicator. A further discussion of the dependence of the results with scale is done in section 3.a.3.

Results obtained for both reanalysis are consistent with each other, as can be checked from Figure 1 (ERA) and Fig. 2 (NCEP), and do not depend on whether one undertakes a yearly average (a,d), or seasonal (b,c,e,f): in the panels (a,b,c), which show height dependence of the longitudinally averaged $\langle \mathscr{D}_\ell(\vec{u},b)\rangle_{long}$, one observes the the total local energy transfers $\mathscr{D}_\ell(\vec{u},b)$ are mostly positive in the troposphere, about zero at the tropopause and negative in the lower stratosphere. By looking at cuts at different pressure levels, one can look more precisely about the spatial distribution of the yearly and seasonal averages of $\langle \mathscr{D}_\ell(\vec{u},b)\rangle_{time}$. Close to the ground ($P = 1000$ hPa), the DR indicator is approximately zero except in proximity of sharp elevation gradients (Antarctica costs, Himalaya, Greenland and Andes mountain ranges). By splitting the local energy transfers is their kinetic $\langle \mathscr{D}_\ell(\vec{u})\rangle_{time}$ and thermodynamic part $\langle \mathscr{D}_\ell^T\rangle_{time}$ (Fig. S1-S4), one sees that this effect is mostly due to the the density fluctuations (i.e. the thermodynamic component of the DR indicator) that produce these negative fluxes.

In the middle troposphere ($P = 500$ hPa), the behavior of $\mathscr{D}_\ell(\vec{u},b)$ is associated to that of the jet stream, since the most intense positive patterns are observed in winter for the northern hemisphere and summer for the southern hemisphere. In the lower stratosphere ($P = 100$ hPa), $\mathscr{D}_\ell(\vec{u},b)$ is negative at the middle latitudes, and become slightly positive in polar regions and in the intertropical convergence zone. Overall, the splitting between the kinetic and thermodynamic component detailed in the Supplementary material suggests that the dynamical component dominates with respect to the thermodynamic one, although the DR thermodynamic contributions are significant especially in the proximity of the ground.

2) CORRELATION WITH ENERGY SPECTRUM

The above result shows that the kinetic energy flux are globally positive in the troposphere, indicating a *direct* kinetic energy cascade, while they are negative in the lower stratosphere indicating a *inverse* kinetic energy cascade. Our results are therefore consistent with those found by Peng et al. (2015) who also found upscale transfer in the lower stratosphere at outer mesoscale length scales and downscale transfers at scales smaller than 360 km (KE) or 200 km (APE).

To get some insight on these cascades, we have further computed the kinetic horizontal energy spectra where k is the inverse of the wavelength from the horizontal velocity fields at different pressure levels in the two reanalysis. They are reported in Figure 5. One sees that for $P \leq 500$ hPa (corresponding to the stratosphere), the energy spectrum is mostly scaling like k^{-3}, while for $P \geq 500$ hPa (middle troposphere), the energy spectrum scales like $k^{-5/3}$, at least for scales larger than $\ell = 220$ km-in agreement with the Nastrom-Gage spectrum in the lower stratosphere at scales between 10^3 and 10^2 km. In the ERA Interim data, the spectrum steepens below this scale and is closer to k^{-2}. These values are however to be taken with caution, since our resolution does not able one to distinguish clearly between a slope of $-5/3$ and $-7/5$ or $-11/5$ and -3, which are classical spectral slope that appear in rotating stratified or quasi 2D turbulence. The difference in spectra between the troposphere and stratosphere can be explained by different values of ratio of f the rotation frequency, to N the Brunt-Vaissala frequency, that was shown to influence strongly the spectral slope and the magnitude or sign of the energy transfer (Pouquet et al. 2017). By changing the value of f/N, one may also change the value of the crossover between the large scales involving an inverse energy cascade, and the small scale, involving a direct energy cascade.

3) Probability distribution functions of instantaneous local energy transfers

In addition to time average, it is also interesting to study the probability distribution function of instantaneous local energy transfers, $\mathscr{D}_\ell(\vec{u},b)$ at a different height (pressure level), and see how it varies with scale and height. This is provided in Figure 3 for ERA-Interim and Figure 4 for NCAR reanalyses. Panels (b,d,f) show the distributions at each level for $\ell = 220$ km. Panels (a,b) show the kinetic component $\mathscr{D}_\ell(\vec{u},0)$, panels (c,d) the thermodynamic component $\mathscr{D}_\ell^T$ and (e,f) the total $\mathscr{D}_\ell(\vec{u},b)$. Tables S1 ans S2 of the supplemental material report the values of mean, standard deviation, skewness and kurtosis as a function of the height for the total DR indicator.

Overall, all distributions are skewed, and exhibit fat tails. The sign of the skewness depends on the height: for both the total and kinetic component, it is positive in the lower troposphere, and negative for $P < 500$ hPa, in agreement with the time averages. For the thermodynamic part, the behaviour is opposite, with a negative skewness at low altitude ($P > 700hPa$) and positive skewness at large altitude. In such case, the distribution is totally asymmetric, and includes only positive transfer, indicating that in the high part of the atmosphere, the density fluctuations only contribute to a downscale energy transfer. Although there is agreement between the ERA interim and the NCEP-NCAR data, the latter shows fatter tails. This might be due either to the different resolution of the datasets and/or on the different physical parametrizations.

Looking now at the dependence with scale at fixed height, we see that both the kinetic and total local energy transfer display similar behaviour, with a tendency to have fatter tails with decreasing scales. This means that the energy imbalance of the reanalysis is reduced when we look at motions whose characteristic scales are larger. This type of behaviour was also observed in local energy transfers measured in a laboratory turbulent von Karman flow (Saw et al. 2016), and therefore

appear generic of highly turbulent flows. Regarding the thermodynamical part of the transfer, the scale dependence is much more mild on the positive side of the distribution, and even absent in the negative part of the distribution.

4) POSSIBLE INTERPRETATION

A possible way to explain the sign of the DR indicatoris to invoke the relation between baroclinic and barotropic flows and direct and inverse cascades. In Tung and Orlando (2003), it is argued that he baroclinic motions responsible for the genesis and decay of extratropical cyclones are mostly associated to direct cascades (corresponding to positive $\mathscr{D}_\ell(\vec{u},b)$), while the essentially barotropic motions governing the lower stratosphere atmospheric dynamics, are associated to an inverse energy cascade (that would correspond to negative values of $\mathscr{D}_\ell(\vec{u},b)$). To check such interpretation, we have analyzed the maps of $\mathscr{D}_\ell(\vec{u})$ collected each 6 or 12h depending on the datasets. They are collected for NCEP-NCAR in the supplementary video. Large positive and negative values of the DR indicator are found as dipoles in baroclinic eddies. When increasing the scale ℓ of the analysis, the tails become lighter as the local positive and negative contributions get averaged out. To investigate better the role of baroclinic eddies in the development of large, positive, DR values, we analyze two tropical cyclones (Katrina and Jolina) whose life-cycle ended up as extratropical storms.

b. Local energy transfers during two case-studies hurricanes

Some aspects of DR indicator evolution in Katrina and Jolina (Nabi) tropical cyclones case studies are shown in Figures 6,7 and 8. More time snapshots of 3D DR indicator are reported in Figure S5 and S6 of the supplemental material. These extreme events have been well documented in the literature (Wang and Oey 2008; Harr et al. 2008; Hsiao et al. 2009). Here we observe

that hurricanes correspond to large values of the DR indicator and are extremely localized in space and time. To have a finer understanding of their dynamics, we have computed $\mathscr{D}_\ell(\vec{u},b)$ in proximity of the cyclonic structures and we use the dataset at higher resolution (ERA-Interim). Figures 6,7 show a single snapshot where the dynamical $\mathscr{D}_\ell(\vec{u})$ (a), $\mathscr{D}_\ell^T$ thermodynamic (b) and total $\mathscr{D}_\ell(\vec{u},b)$ component (c). At every time step, we have isolated the cyclone as the region bordered by sea-level pressure (SLP) values lower than 1005 hPa (in the case of Katrina), lower than 1000hPa (in the case of Jolina). The threshold difference is motivated by the presence of other low pressure structures in the region corresponding to Jolina's trajectory. As the cyclones follow their path, a transition occurs from a condition characterized by the alternation of negative and positive DR values, to one characterized by dominant positive values. This is particularly evident in the middle levels of the troposphere (between 850 hPa and 250 hPa).

Some relevant differences are found, comparing the two cyclones. On one hand, $\mathscr{D}_\ell(\vec{u},b)$ decreases as Katrina moves northward, and the patterns of DR at higher levels apparently lose their co-variability with the surface structure of the cyclone. On the other hand, the DR indicator remains large as Jolina moves northward, preserving its vertical coherence. Furthermore, the land-sea contrasts seems to have a role in shaping the DR patterns at lower levels, with Jolina possibly deriving its strength from its permanence over a sea surface, even at mid-latitudes. While Katrina loses its energy source as cyclonic system as soon as it move northward in the continental areas, Jolina develops into a powerful extra-tropical storm, as also noticeable looking at the SLP values at the center of the system (Harr et al. 2008).

The DR evolution during the lifetime of the two systems suggests the different natures of energy transfers in a tropical cyclone: Dominant positive $\mathscr{D}_\ell(\vec{u},b)$ values reflect an unresolved energy transfer towards the smaller scales, that is coherent with the downscale enstrophy transfer by

means of eddy-eddy interaction in baroclinic eddies (Burgess et al. 2013). The jet stream, which is sustained by the eddy-mean flow interactions over mid-latitudes, is indeed denoted by large positive DR values (cfr. Figure 1), enforcing the hypothesis that the downscale enstrophy transfer is associated with an upscale kinetic energy transfer (Held and Hoskins 1985; Straus and Ditlevsen 1999). The thermodynamic structure of DR indicator (Panels b in Figure6-7) is interesting because the positive energy transfers in the middle troposphere can be associated to the presence of the warm core of the tropical cyclones, transferring energy to small scale proceses. A dipole vertical structure emerges, as shown in Figure 1, with opposite sign DR values in coincidence of the jet stream. This is consistent with previous findings from general circulation models (Koshyk and Hamilton 2001) and higher resolution reanalysis (Burgess et al. 2013), showing a decay of synoptic scale rotational kinetic energy and a downscale transfer of divergent kinetic energy above the jet stream and in correspondence to the tropopause. As a caveat, hurricanes are associated with strong horizontal divergence and convergence (and generation of kinetic energy) which can affect the interpretation of $\mathscr{D}_\ell(\vec{u},b)$ for such low resolution reanalysis datasets. It will definitely be worth to compare these computations with those obtained at higher spatial and temporal resolutions.

4. Discussion

Weather and climate models do not resolve the viscous scales, which for the atmospheric motions are order of 0.1 mm (Priestley 1959). Up to date, their resolution ranges from $\simeq$ 2 km of regional weather models to $\simeq$ 100 km of global climate models. To correctly represent dissipation effects at a scale ℓ, the turbulent cascade needs to be parametrized at each grid point depending on the type of motion and the geographical constraints. Despite the importance of such energy transfers, their distribution and their time and spatial behavior is known only partially through field campaigns (Lübken 1997) or by global averages (Sellers 1969; Seinfeld and Pandis 2016). This

does not ensure a global coverage and does not tell the direction of the energy transfers in the free troposphere. In this paper, we have used Duchon and Robert (2000) to compute and characterize the distribution of instantaneous and local sub-filter energy transfers in the atmosphere using 3D velocity fields obtained in NCEP-NCAR and ERA-Interim reanalysis. Those energy transfers are highly correlated with the baroclinic eddies occurring at mid-latitudes and with severe tropical cyclones. Our computation of local energy transfer provides the direction of the local energy cascade at a certain scale ℓ in physical space. At the grid resolution l, the value of $\mathscr{D}_\ell(\vec{u},b)$ is an exact measure of the amount of energy *that must be transferred to subgrid scales* (positive DR contributions) or *that must be injected from the subgrid scales* (negative contributions) to the scale ℓ of the analysis. This information could be used to interactively adjust the energy fluxes to account for the energy conservation laws in the atmosphere (Lucarini and Ragone 2011). Furthermore, the expression of $\mathscr{D}_\ell(\vec{u})$ is separable in a dynamical and a thermodynamic contributions. Although most of the total $\mathscr{D}_\ell(\vec{u},b)$ contribution is due to the dynamical component, negative fluxes are found at the ground in presence of mountain ranges and sharp temperature/pressure gradients, positive fluxes in the middle troposphere reinforce the dynamic contrbutions. We have also observed that extreme events as tropical and extratropical storms are associated with large values of $\mathscr{D}_\ell(\vec{u},b)$, even at the ground.

The quantity $\mathscr{D}_\ell(\vec{u},b)$ could also be a proxy of the flux of energy that can be exploited in wind turbines (Miller et al. 2011, 2015). Although our analysis is performed for large scale general circulation models, the Duchon and Robert (2000) formula can be applied to regional climate and weather prediction models. At smaller scales, it will be extremely interesting to analyze the relation between $\mathscr{D}_\ell(\vec{u},b)$ and the genesis of extreme wind gusts or even tornadoes. At such scales, one could investigate the distributions of $\mathscr{D}_\ell(\vec{u},b)$ to the instantaneous subgrid scales dissipation obtained by field measurements (Higgins et al. 2003). It will also been worth to investigate whether

adaptive asymptotic methods, as those proposed by Klein et al. (2001) or the Lagrangian scale-dependant models for the subgrid scales in Large Eddy Simulations (Bou-Zeid et al. 2004), afford better energy balances, i.e. the spatial and temporal average of $\mathscr{D}_\ell(\vec{u},b)$ is closer to zero.

It is evident that the resolution plays an important role in determining spurious energy fluxes by looking at the difference in the $\mathscr{D}_\ell(\vec{u},b)$ indicator near the ground (NCAR vs ERA-Interim reanalysis). However, it is positively surprising that the average spatial and vertical structure of the indicators is very similar in both reanalysis.

Several waves phenomena in the atmospheric - gravity and Rossby waves - are tied to these horizontal density variations, and are associated with energy conversion between available potential and kinetic energy. One key question is whether this diagnostic may incorrectly assess such energy conversion as an energy transfer across scale. For future research directions, it might be worth applying the diagnostic to a simple gravity or Rossby wave model.

APPENDIX

A1. Derivation of the local Duchon-Robert equation for Boussinesq equations

We start from the Boussinesq equation Eqs. (2) for the buoyancy perturbation and write it at two different position, $\vec{x}$ and $\vec{x}'$ for $b(\vec{x})$ and $b' = b(\vec{x}')$ and $u(\vec{x})$ and $u' = u(\vec{x}')$:

$$\partial_t b + \partial_j(u_j b) = -N^2 u_z + \kappa \partial_j^2 b, \tag{A1}$$

$$\partial_t b' + \partial_j(u'_j b') = -N^2 u'_z + \kappa \partial_j^2 b', \tag{A2}$$

Multiplying the equation (A1) by b' and equation (A2) by b and adding the results we obtain

$$\partial_t(bb') + b\partial_j(b'u'_j) + b'\partial_j(bu_j) = -N^2\left(b'u_z + bu'_z\right) + \kappa\left(b'\partial_j^2 b + b\partial_j^2 b'\right) \ . \tag{A3}$$

To simplify the equation, we can write the diffusive term as

$$b'\partial_j^2 b + b\partial_j^2 b' = \partial_j^2 bb' - 2\partial_j b\partial_j b' \ , \tag{A4}$$

while the nonlinear can be written as

$$b\partial_j b' u'_j + b'\partial_j b u_j = b\delta u_j \partial_j b' + \partial_j b u_j b' \ , \tag{A5}$$

where $\delta u_j = u'_j - u_j$ as before. Considering the term $(u'_j - u_j)(b' - b)^2 = \delta u_j (\delta b)^2$, it reads as

$$\delta u_j (\delta b)^2 = b'^2(\delta u_j) + b^2(\delta u_j) - 2b'(u'_j - u_j)b \tag{A6}$$

Using now the identities $\nabla_r \cdot (\delta \mathbf{u}) = \nabla_r \cdot \mathbf{u}' = 0$, and after some manipulations we have:

$$b\delta u_j \partial_j b' = \frac{1}{2}\left[\partial_j (b'^2 \delta u_j) - \partial_j (\delta u_j (\delta b)^2)\right] + \partial_j b u_j b' \tag{A7}$$

Substituting the results from the equations (A4) and (A7) and multiplying both the sides by $1/2$ and simplifying gives:

$$\partial_t (\frac{1}{2} bb') + \frac{1}{2}\partial_j \left((u_j b')b + \frac{1}{2} b'^2 \delta u_j - \kappa \partial_j (bb') \right) = \frac{1}{4}\nabla_r \cdot \delta\vec{u} (\delta b)^2 - \kappa \partial_j b \partial_j b' - \frac{N^2}{2}\left(b u'_z + b' u_z \right) \ ; \tag{A8}$$

Applying the filter operator G_ℓ, and noting $\hat{f} = f * G_\ell$ ($*$ being the convolution), we get:

$$\begin{aligned} \partial_t (\frac{1}{2} b\hat{b}) \ &+ \ \vec{\nabla} \cdot \left(\frac{1}{2}(\vec{u}\hat{b})b + \frac{1}{4}\widehat{(b^2\vec{u})} - \frac{1}{4}\widehat{(b^2)}\vec{u} - \kappa\vec{\nabla}(\frac{1}{2} b\hat{b}) \right) \\ &= \ -\frac{1}{4\ell}\int d\vec{r} (\vec{\nabla} G)_l \cdot \delta\vec{u}(r)(\delta b)^2 - \kappa \vec{\nabla} b \cdot \vec{\nabla}\hat{b} - \frac{N^2}{2}\left(b\hat{u}_z + \hat{b} u_z \right). \end{aligned} \tag{A9}$$

Introducing $E_T^\ell = b\hat{b}/2N^2$,the available potential energy at scale ℓ , and the terms

$$\vec{J}_T^\ell \ = \ \left(\frac{1}{2}(\vec{u}\hat{b})b + \frac{1}{4}\widehat{(b^2\vec{u})} - \frac{1}{4}\widehat{(b^2)}\vec{u} - \kappa\vec{\nabla}(\frac{1}{2} b\hat{b}) \right)/N^2, \tag{A10}$$

$$\mathscr{D}_\ell^b \ = \ \frac{1}{4l}\int d^d r (\vec{\nabla} G)_l \cdot \delta\vec{u}(r)(\delta b)^2/N^2, \tag{A11}$$

we get the equation , Eq (9) of section 2.

Now, taking the limit $\ell \to 0$ and introducing the available potential energy $E_T = b^2/2N^2$, the equation finally simplifies to:

$$\partial_t E_T + \vec{\nabla}\cdot(\frac{1}{2}\vec{u}E_T) - \kappa\nabla^2 E_T = -bu_z - \mathscr{D}^b - \kappa(\nabla b)^2/N^2, \tag{A12}$$

with

$$\mathscr{D}^b = \lim_{l\to 0}\mathscr{D}^b_\ell. \tag{A13}$$

The equation for the kinetic energy has been derived in Duchon and Robert (2000), without the term due to buoyancy which can be simply included, and writes as:

$$\begin{aligned}\partial_t E^\ell \;&+\; \partial_j\left(\hat{u}_j E^\ell + \frac{1}{2}\left(u_j\hat{p} + \hat{u}_j p\right) + \frac{1}{4}\left(\widehat{u^2 u_j} - \frac{1}{4}\widehat{u^2}u_j\right) - \nu\partial_j E^\ell\right) = \\ &-\; \nu\partial_j u_i \partial_j \hat{u}_i - \mathscr{D}_\ell + \frac{1}{2}\left(b\hat{u}_z + \hat{b}u_z\right),\end{aligned} \tag{A14}$$

with $\mathscr{D}_\ell$ being given by Eq. 6. Introducig the KE spatial flux:

$$\vec{J}^\ell_K = \hat{\vec{u}}E^\ell + \frac{1}{2}\left(\vec{u}\hat{p} + \hat{\vec{u}}p\right) + \frac{1}{4}\left(\widehat{(u^2\vec{u})} - \frac{1}{4}\widehat{(u^2)}\vec{u}\right) - \nu\vec{\nabla}E^\ell, \tag{A15}$$

we get Eq. (8) of section 2.

Acknowledgments. D. Faranda was supported by ERC grant No. 338965. DF thanks G. Messori and N. Vercauteren for useful discussions and comments on the paper.

References

Augier, P., S. Galtier, and P. Billant, 2012: Kolmogorov laws for stratified turbulence. *Journal of Fluid Mechanics*, **709**, 659–670.

Augier, P., and E. Lindborg, 2013: A new formulation of the spectral energy budget of the atmosphere, with application to two high-resolution general circulation models. *Journal of the Atmospheric Sciences*, **70 (7)**, 2293–2308.

Bartello, P., 1995: Geostrophic adjustment and inverse cascades in rotating stratified turbulence. *Journal of the atmospheric sciences*, **52 (24)**, 4410–4428.

Beljaars, A., 1995: The parametrization of surface fluxes in large-scale models under free convection. *Quarterly Journal of the Royal Meteorological Society*, **121 (522)**, 255–270.

Berrisford, P., P. Kållberg, S. Kobayashi, D. Dee, S. Uppala, a. J. Simmons, P. Poli, and H. Sato, 2011: Atmospheric conservation properties in ERA-Interim. *Quarterly Journal of the Royal Meteorological Society*, **137 (July)**, 1381–1399, doi:10.1002/qj.864.

Bou-Zeid, E., C. Meneveau, and M. B. Parlange, 2004: Large-eddy simulation of neutral atmospheric boundary layer flow over heterogeneous surfaces: Blending height and effective surface roughness. *Water Resources Research*, **40 (2)**.

Brunke, M. A., Z. Wang, X. Zeng, M. Bosilovich, and C.-L. Shie, 2011: An assessment of the uncertainties in ocean surface turbulent fluxes in 11 reanalysis, satellite-derived, and combined global datasets. *Journal of Climate*, **24 (21)**, 5469–5493.

Burgess, B. H., A. R. Erler, and T. G. Shepherd, 2013: The troposphere-to-stratosphere transition in kinetic energy spectra and nonlinear spectral fluxes as seen in ecmwf analyses. *Journal of the Atmospheric Sciences*, **70 (2)**, 669–687.

Cao, C., S. Ibrahim, K. Nakanishi, and E. S. Titi, 2015: Finite-time blowup for the inviscid primitive equations of oceanic and atmospheric dynamics. *Communications in Mathematical Physics*, **337 (2)**, 473–482.

Cao, C., and E. S. Titi, 2007: Global well-posedness of the three-dimensional viscous primitive equations of large scale ocean and atmosphere dynamics. *Annals of Mathematics*, 245–267.

Charney, J. G., 1971: Geostrophic turbulence. *Journal of the Atmospheric Sciences*, **28 (6)**, 1087–1095.

Dee, D. P., and Coauthors, 2011: The ERA-Interim reanalysis: configuration and performance of the data assimilation system. *Quarterly Journal of the Royal Meteorological Society*, **137 (656)**, 553–597, doi:10.1002/qj.828, URL http://doi.wiley.com/10.1002/qj.828.

Duchon, J., and R. Robert, 2000: Inertial energy dissipation for weak solutions of incompressible euler and navier-stokes equations. *Nonlinearity*, **13 (1)**, 249.

Falkovich, G., 1992: Inverse cascade and wave condensate in mesoscale atmospheric turbulence. *Physical review letters*, **69 (22)**, 3173.

Frisch, U., 1995: *Turbulence: the legacy of AN Kolmogorov*. Cambridge university press.

Gage, K., 1979: Evidence far ak- 5/3 law inertial range in mesoscale two-dimensional turbulence. *Journal of the Atmospheric Sciences*, **36 (10)**, 1950–1954.

Harr, P. A., D. Anwender, and S. C. Jones, 2008: Predictability associated with the downstream impacts of the extratropical transition of tropical cyclones: Methodology and a case study of typhoon nabi (2005). *Monthly Weather Review*, **136 (9)**, 3205–3225.

Held, I. M., and B. J. Hoskins, 1985: Large-scale eddies and the general circulation of the troposphere. *Advances in Geophysics*, **28**, 3–31.

Higgins, C. W., M. B. Parlange, and C. Meneveau, 2003: Alignment trends of velocity gradients and subgrid-scale fluxes in the turbulent atmospheric boundary layer. *Boundary-Layer Meteorology*, **109 (1)**, 59–83.

Holton, J. R., and G. J. Hakim, 2012: *An introduction to dynamic meteorology*, Vol. 88. Academic press.

Hsiao, L.-F., M. S. Peng, D.-S. Chen, K.-N. Huang, and T.-C. Yeh, 2009: Sensitivity of typhoon track predictions in a regional prediction system to initial and lateral boundary conditions. *Journal of Applied Meteorology and Climatology*, **48 (9)**, 1913–1928.

Kalnay, E., and Coauthors, 1996: The NCEP/NCAR 40-year reanalysis project. *Bulletin of the American Meteorological Society*, **77**, 437–471, doi:10.1175/1520-0477(1996)077⟨0437:TNYRP⟩2.0.CO;2.

Kitamura, Y., and Y. Matsuda, 2006: The kh- 3 and kh- 5/3 energy spectra in stratified turbulence. *Geophysical research letters*, **33 (5)**.

Klein, R., 2010: Scale-dependent models for atmospheric flows. *Annual review of fluid mechanics*, **42**, 249–274.

Klein, R., N. Botta, T. Schneider, C.-D. Munz, S. Roller, A. Meister, L. Hoffmann, and T. Sonar, 2001: Asymptotic adaptive methods for multi-scale problems in fluid mechanics. *Practical Asymptotics*, Springer, 261–343.

Kolmogorov, A. N., 1941: Dissipation of energy in locally isotropic turbulence. *Dokl. Akad. Nauk SSSR*, Vol. 32, 16–18.

Koshyk, J. N., and K. Hamilton, 2001: The horizontal kinetic energy spectrum and spectral budget simulated by a high-resolution troposphere-stratosphere-mesosphere gcm. *Journal of the atmospheric sciences*, **58 (4)**, 329–348.

Kuzzay, D., D. Faranda, and B. Dubrulle, 2015: Global vs local energy dissipation: The energy cycle of the turbulent von kármán flow. *Physics of Fluids (1994-present)*, **27 (7)**, 075 105.

Levich, E., and E. Tzvetkov, 1985: Helical inverse cascade in three-dimensional turbulence as a fundamental dominant mechanism in mesoscale atmospheric phenomena. *Physics reports*, **128 (1)**, 1–37.

Lilly, D. K., 1983: Stratified turbulence and the mesoscale variability of the atmosphere. *Journal of the Atmospheric Sciences*, **40 (3)**, 749–761.

Lindborg, E., 2005: The effect of rotation on the mesoscale energy cascade in the free atmosphere. *Geophysical research letters*, **32 (1)**.

Lindborg, E., 2006: The energy cascade in a strongly stratified fluid. *Journal of Fluid Mechanics*, **550**, 207–242.

Lindborg, E., and J. Y. Cho, 2001: Horizontal velocity structure functions in the upper troposphere and lower stratosphere. ii- theoretical considerations. *Journal of geophysical research*, **106**, 10.

Lorenz, E. N., 1955: Available potential energ and the maintenance of the general. *Tellus*, **7**, 2.

Lovejoy, S., and D. Schertzer, 2010: Towards a new synthesis for atmospheric dynamics: space–time cascades. *Atmospheric Research*, **96 (1)**, 1–52.

Lübken, F.-J., 1997: Seasonal variation of turbulent energy dissipation rates at high latitudes as determined by in situ measurements of neutral density fluctuations. *Journal of Geophysical Research: Atmospheres*, **102 (D12)**, 13 441–13 456.

Lucarini, V., and F. Ragone, 2011: Energetics of climate models: Net energy balance and meridional enthalpy transport. *Reviews of Geophysics*, **49 (1)**.

Miller, L. M., N. A. Brunsell, D. B. Mechem, F. Gans, A. J. Monaghan, R. Vautard, D. W. Keith, and A. Kleidon, 2015: Two methods for estimating limits to large-scale wind power generation. *Proceedings of the National Academy of Sciences*, **112 (36)**, 11 169–11 174.

Miller, L. M., F. Gans, and A. Kleidon, 2011: Estimating maximum global land surface wind power extractability and associated climatic consequences. *Earth Syst. Dynam*, **2 (1)**, 1–12.

Miyakoda, K., and J. Sirutis, 1986: Manual of the e-physics. *Available from Geophysical Fluid Dynamics Laboratory, Princeton University, PO Box*, **308**.

Nastrom, G., and K. S. Gage, 1985: A climatology of atmospheric wavenumber spectra of wind and temperature observed by commercial aircraft. *Journal of the atmospheric sciences*, **42 (9)**, 950–960.

Parrish, D. F., and J. C. Derber, 1992: The national meteorological center's spectral statistical-interpolation analysis system. *Monthly Weather Review*, **120 (8)**, 1747–1763, doi:10.1175/1520-0493(1992)120⟨1747:TNMCSS⟩2.0.CO;2, URL http://dx.doi.org/10.1175/1520-0493(1992)120⟨1747:TNMCSS⟩2.0.CO;2.

Peng, J., L. Zhang, and J. Guan, 2015: Applications of a moist nonhydrostatic formulation of the spectral energy budget to baroclinic waves. part i: The lower-stratospheric energy spectra. *Journal of the Atmospheric Sciences*, **72 (5)**, 2090–2108.

Pouquet, A., and R. Marino, 2013: Geophysical turbulence and the duality of the energy flow across scales. *Physical review letters*, **111 (23)**, 234 501.

Pouquet, A., R. Marino, P. D. Mininni, and D. Rosenberg, 2017: Dual constant-flux energy cascades to both large scales and small scales. *Physics of Fluids*, **29 (11)**, 111 108.

Priestley, C. H. B., 1959: *Turbulent transfer in the lower atmosphere*. University of Chicago Press Chicago.

Saw, E.-W., D. Kuzzay, D. Faranda, A. Guittonneau, F. Daviaud, C. Wiertel-Gasquet, V. Padilla, and B. Dubrulle, 2016: Experimental characterization of extreme events of inertial dissipation in a turbulent swirling flow. *Nature Communications*, **7**, 12 466.

Schertzer, D., S. Lovejoy, F. Schmitt, Y. Chigirinskaya, and D. Marsan, 1997: Multifractal cascade dynamics and turbulent intermittency. *Fractals*, **5 (03)**, 427–471.

Seinfeld, J. H., and S. N. Pandis, 2016: *Atmospheric chemistry and physics: from air pollution to climate change*. John Wiley & Sons.

Sellers, W. D., 1969: A global climatic model based on the energy balance of the earth-atmosphere system. *Journal of Applied Meteorology*, **8 (3)**, 392–400.

Smagorinsky, J., 1963: General circulation experiments with the primitive equations: I. the basic experiment*. *Monthly weather review*, **91 (3)**, 99–164.

Stevens, B., and S. Bony, 2013: What are climate models missing? *Science*, **340 (6136)**, 1053–1054.

Straus, D. M., and P. Ditlevsen, 1999: Two-dimensional turbulence properties of the ecmwf reanalyses. *Tellus A*, **51 (5)**, 749–772, doi:10.1034/j.1600-0870.1996.00015.x, URL http://dx.doi.org/10.1034/j.1600-0870.1996.00015.x.

Tang, C. K., and J. C. Chan, 2015: Idealized simulations of the effect of local and remote topographies on tropical cyclone tracks. *Quarterly Journal of the Royal Meteorological Society*, **141 (691)**, 2045–2056.

Tung, K. K., and W. W. Orlando, 2003: The k- 3 and k- 5/3 energy spectrum of atmospheric turbulence: Quasigeostrophic two-level model simulation. *Journal of the atmospheric sciences*, **60 (6)**, 824–835.

Viterbo, P., and A. C. Beljaars, 1995: An improved land surface parameterization scheme in the ecmwf model and its validation. *Journal of Climate*, **8 (11)**, 2716–2748.

Viterbo, P., and A. K. Betts, 1999: Impact on ecmwf forecasts of changes to the albedo of the boreal forests in the presence of snow. *Journal of Geophysical Research: Atmospheres*, **104 (D22)**, 27 803–27 810.

Wang, D.-P., and L.-Y. Oey, 2008: Hindcast of waves and currents in hurricane katrina. *Bulletin of the American Meteorological Society*, **89 (4)**, 487–495.

LIST OF FIGURES

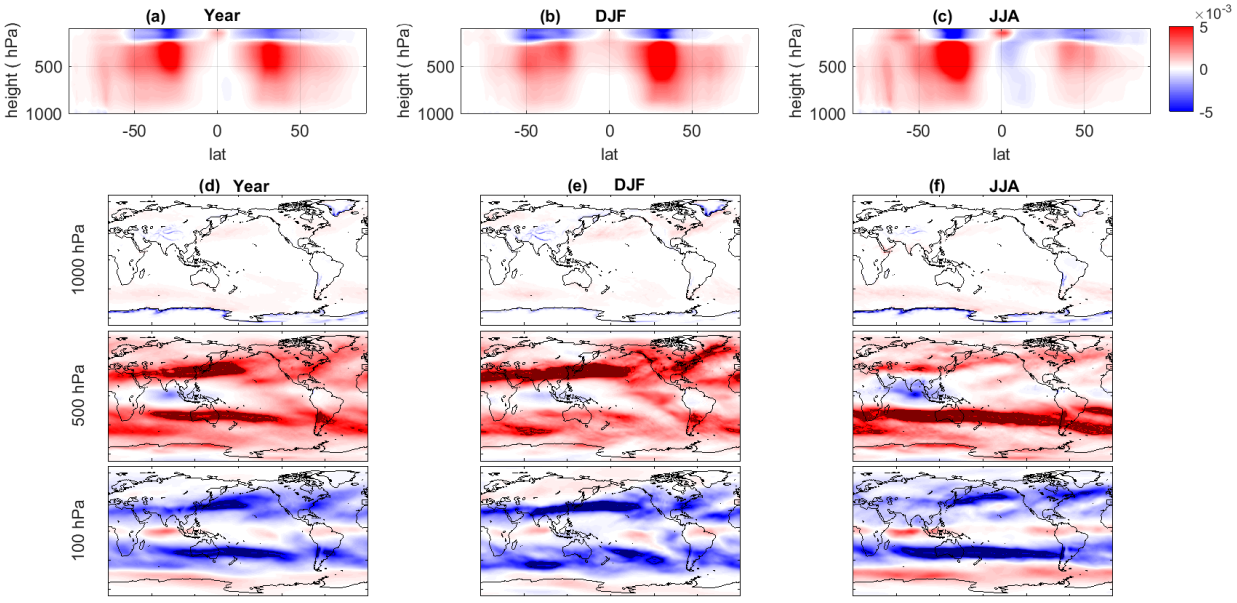

601 FIG. 1. Distribution of $\mathscr{D}_\ell(\vec{u}, b)$ for $\ell = 220$ Km and the ERA-Interim reanalysis. (a-c) longitudinal averages,
602 (d-e-f) maps at three different fixed height: 1000 hPa, 500 hPa and 100hPa. (a,d) yearly averages, (b,e) winter
603 averages, (c,f) summer averages.

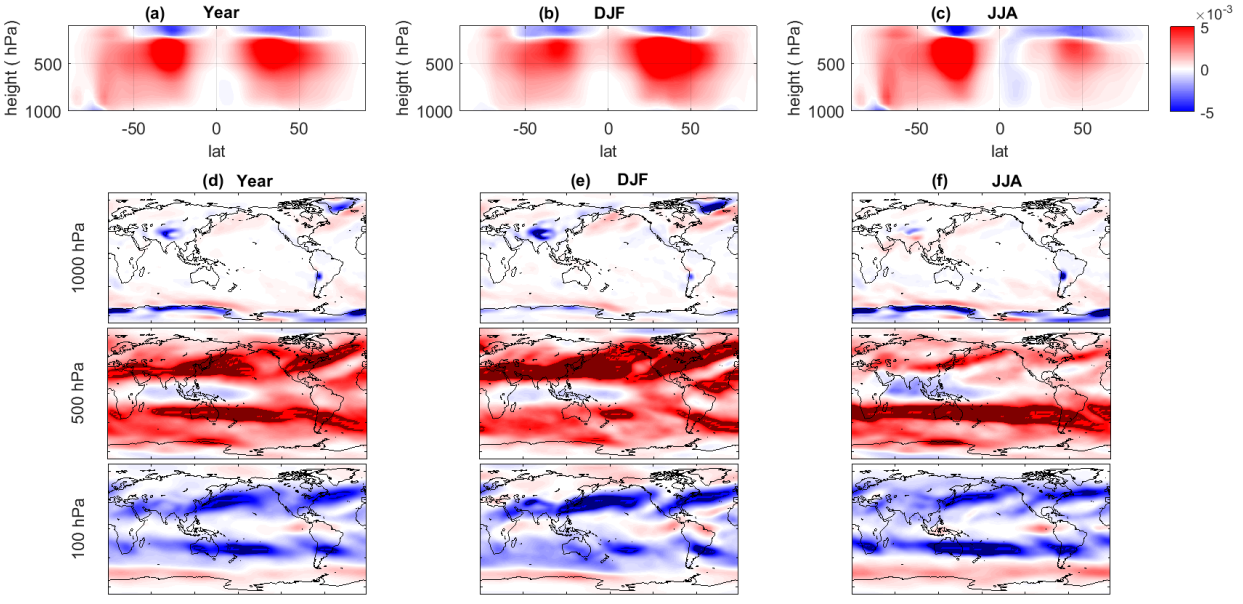

FIG. 2. Distribution of $\mathscr{D}_\ell(\vec{u},b)$ for $\ell = 220$ Km and the NCAR reanalysis. (a-c) longitudinal averages, (d-e-f) maps at three different fixed height: 1000 hPa, 500 hPa and 100hPa. (a,d) yearly averages, (b,e) winter averages, (c,f) summer averages.

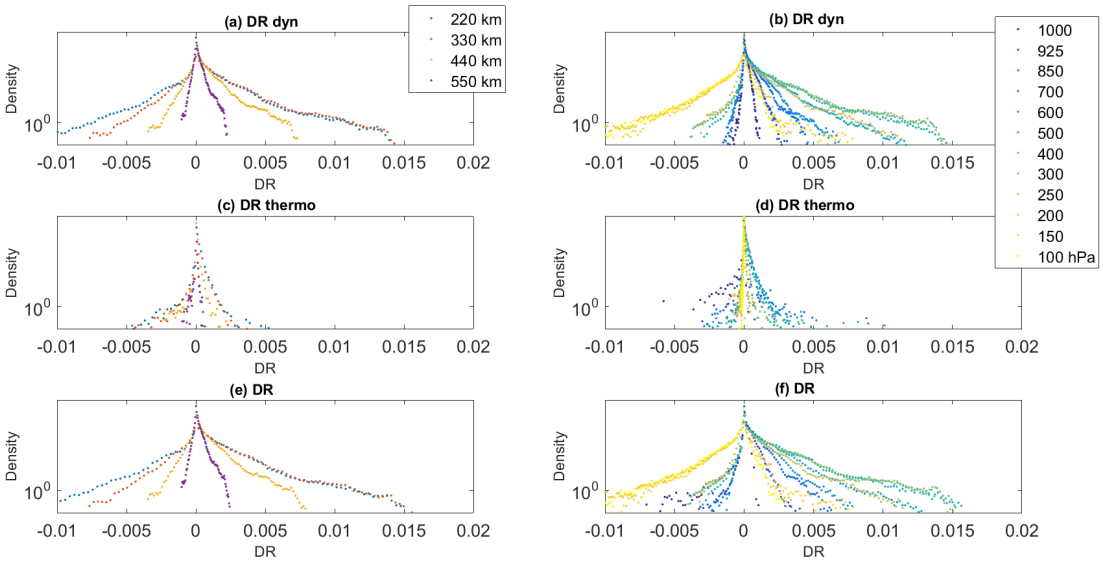

FIG. 3. Empirical $\mathscr{D}_\ell(\vec{u},b)$ density functions for ERA-Interim against scale ℓ of analysis (a,c,e) or height for $\ell = 220$ km (b,d,f). (a,b) panels show the dynamical $\mathscr{D}_\ell(\vec{u})$ component, (c,d) the thermodynamic $\mathscr{D}_\ell^T$ component and (e,f) the total $\mathscr{D}_\ell(\vec{u})$.

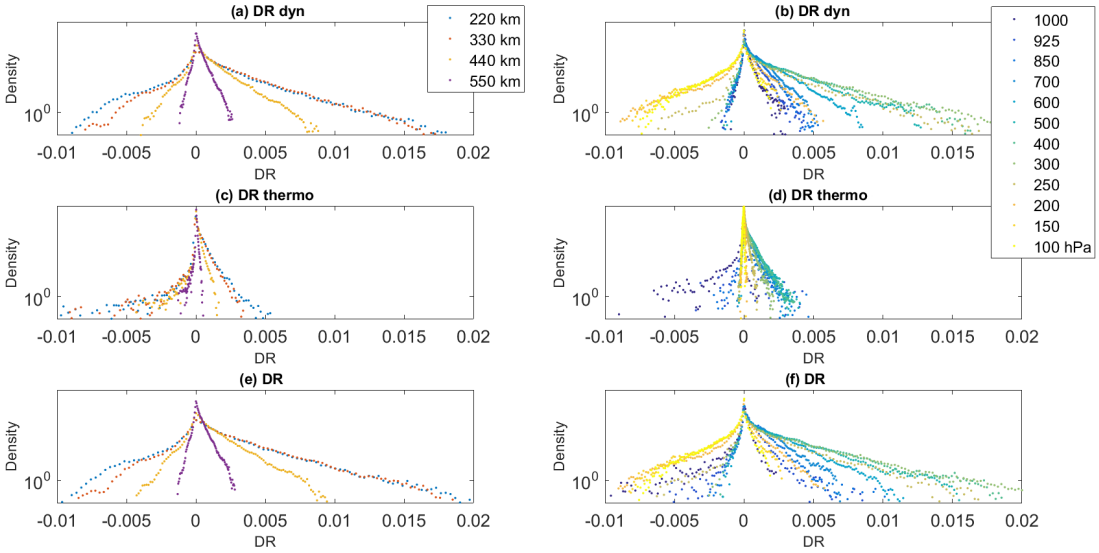

FIG. 4. Empirical $\mathscr{D}_\ell(\vec{u})$ density functions for NCAR reanalysis against scale ℓ of analysis (a,c,e) or height for $\ell = 220$ km (b,d,f). (a,b) panels show the dynamical $\mathscr{D}_\ell(\vec{u})$ component, (c,d) the thermodynamic $\mathscr{D}_\ell^T$ component and (e,f) the total $\mathscr{D}_\ell(\vec{u})$.

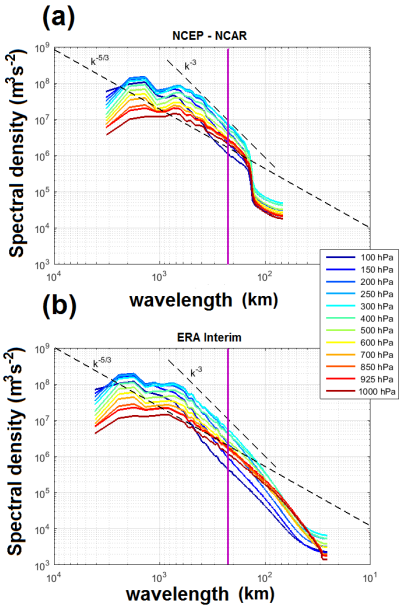

FIG. 5. Solid lines: spectra $E(k)$, where k is the wavelength) computed, at each pressure level, for the horizontal velocity fields. Dotted lines: -5/3 and -3 slopes. Magenta vertical lines: $\ell = 220$ Km. (a): NCEP-NCAR reanalysis, (b): ERA Interim reanalysis.

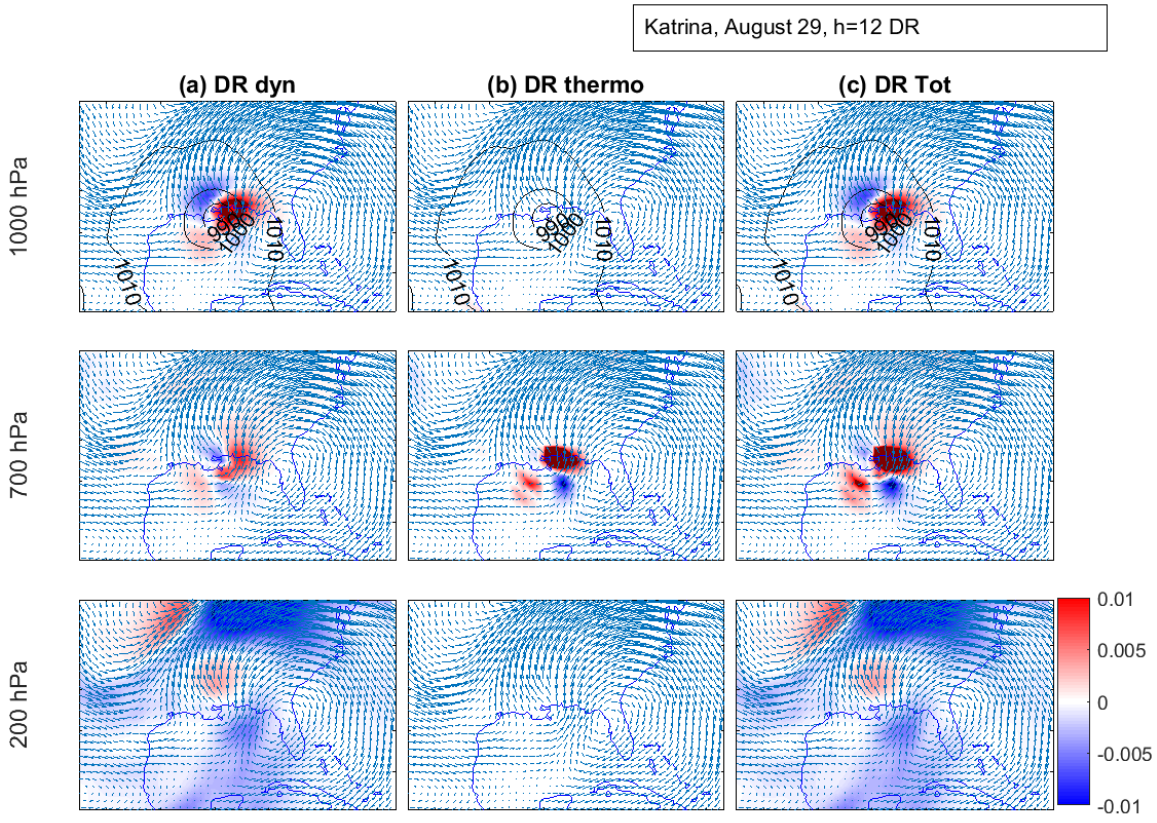

FIG. 6. Katrina Analysis: The maps show $\mathscr{D}_\ell(\vec{u})$ dynamical (a), $\mathscr{D}_\ell^T$ thermodynamic (b) and $\mathscr{D}_\ell(\vec{u},b)$ total (c) components for three different levels (1000,700 and 200 hPa) on August 29th at midday. The arrows size is proportional to the intensity of the horizontal wind. ERA-Interim reanalysis, $\ell = 220$ km.

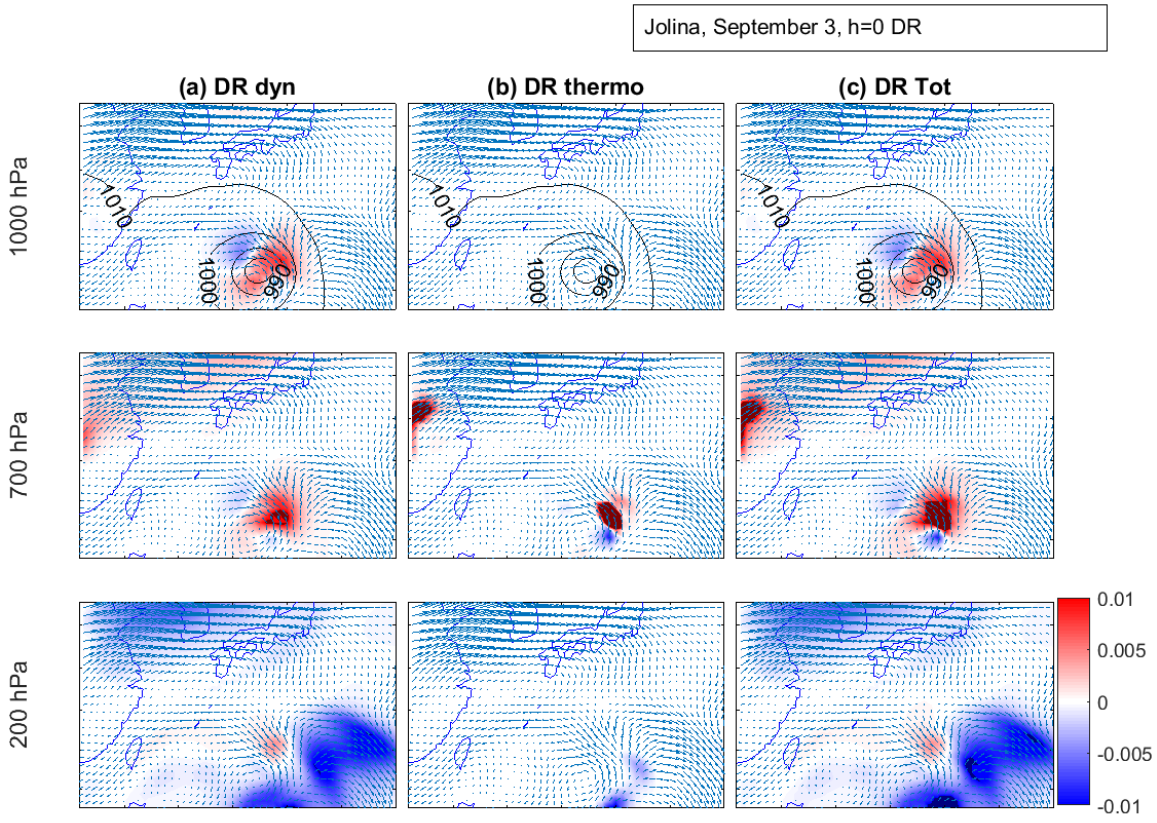

FIG. 7. Jolina Analysis: The maps show $\mathscr{D}_\ell(\vec{u})$ dynamical (a), $\mathscr{D}_\ell^T$ thermodynamic (b) and $\mathscr{D}_\ell(\vec{u},b)$ total (c) components for three different levels (1000,700 and 200 hPa) on August 29th at midday. The arrows size is proportional to the intensity of the horizontal wind. ERA-Interim reanalysis, $\ell = 220$ km.

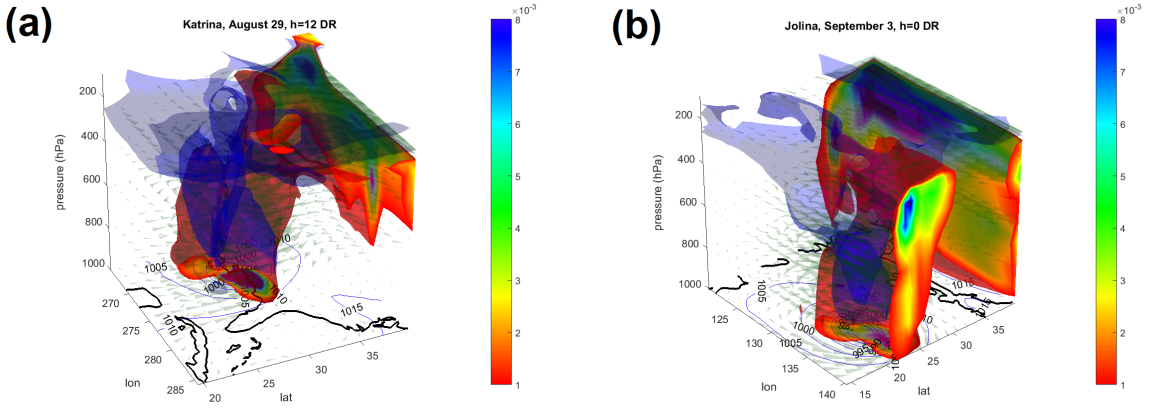

FIG. 8. 3D structure of the wind field (green cones) and $\mathscr{D}_\ell(\vec{u},b)$ for the Hurricane Katrina (a) and Jolina (b), obtained by the ERA-Interim reanalysis, for $\ell = 220$ km. Red: isosurfaces at $\mathscr{D}_\ell(\vec{u}) = 0.001$. Dark Blue: isosurfaces at $\mathscr{D}_\ell(\vec{u}) = -0.001$. The colorscale indicates values $\mathscr{D}_\ell(\vec{u}) > 0.001$. See supplemental material for time evolutions.